ACS SENSORS

pubs.acs.org/acssensors

Article

Elucidating the Mechanisms Underlying the Signal Drift of Electrochemical Aptamer-Based Sensors in Whole Blood

Kaylyn K. Leung, Alex M. Downs, Gabriel Ortega, Martin Kurnik, and Kevin W. Plaxco*

Cite This: *ACS Sens.* 2021, 6, 3340−3347

Read Online

ACCESS | Metrics & More | Article Recommendations | Supporting Information

ABSTRACT: The ability to monitor drugs, metabolites, hormones, and other biomarkers in situ in the body would greatly advance both clinical practice and biomedical research. To this end, we are developing electrochemical aptamer-based (EAB) sensors, a platform technology able to perform real-time, in vivo monitoring of specific molecules irrespective of their chemical or enzymatic reactivity. An important obstacle to the deployment of EAB sensors in the challenging environments found in the living body is signal drift, whereby the sensor signal decreases over time. To date, we have demonstrated a number of approaches by which this drift can be corrected sufficiently well to achieve good measurement precision over multihour in vivo deployments. To achieve a much longer in vivo measurement duration, however, will likely require that we understand and address the sources of this effect. In response, here, we have systematically examined the mechanisms underlying the drift seen when EAB sensors and simpler, EAB-like devices are challenged in vitro at 37 °C in whole blood as a proxy for in vivo conditions. Our results demonstrate that electrochemically driven desorption of a self-assembled monolayer and fouling by blood components are the two primary sources of signal loss under these conditions, suggesting targeted approaches to remediating this degradation and thus improving the stability of EAB sensors and other, similar electrochemical biosensor technologies when deployed in the body.

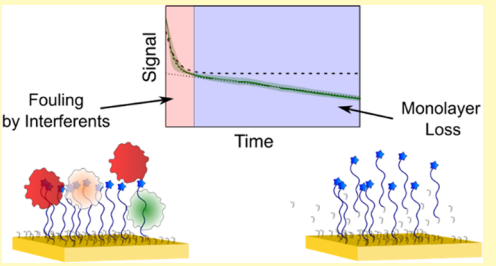

KEYWORDS: *electrochemical DNA biosensor, stability, self-assembled monolayers, electrodes, fouling*

An ability to monitor the in-body levels of clinically relevant molecular targets, including hormones, biomarkers, drugs, and metabolites, would significantly advance both biomedical research and personalized medicine. As a means to this end, we and others have developed electrochemical biosensors employing redox-reporter-modified, electrode-bound deoxyribonucleic acid (DNA) or DNA-polypeptide/protein/small molecule conjugates that are capable of measuring the levels of specific molecular targets in complex clinical sample matrices.[1−5] These include electrochemical aptamer-based (EAB) sensors, which are comprised of a redox-reporter-modified DNA aptamer attached to an interrogating electrode (Figure 1A) and support the high-frequency measurement of specific molecules in situ in the living body.[1,6,7] For example, we have used micron-diameter, millimeter-long EAB sensors to perform seconds-resolved measurements of more than a half-dozen therapeutics, drugs of abuse, and metabolites in situ within the circulatory system and tissues of live rats.[1,6,8,9] The availability of such real-time molecular measurements has enabled new applications, including close-loop, feedback-controlled drug delivery,[6,7] which could usher in an unprecedented new era of high-precision therapeutics.[10]

When EAB sensors are deployed in the harsh conditions found in the body, their signal drifts (Figure 1B). To rectify this, we typically employ empirical drift correction methods,[11,12] in which the changing electrochemical signal is normalized (Figure 1C), for example, to a standardizing signal generated at a second square-wave frequency.[11,12] Using such approaches, we achieve good measurement precision over many-hour measurement runs in live animals.[1] Unfortunately, however, no matter how accurate it is, drift correction must eventually fail when the sensor's signaling current—and thus its signal-to-noise ratio—falls arbitrarily low, ultimately limiting the duration of in vivo measurements.[1] Given this, we explore here the mechanisms by which EAB sensors degrade with the expectation that an improved understanding of these mechanisms will suggest methods of extending the measurement duration.

RESULTS

To date, four mechanisms have been proposed to underly the degradation of EAB sensors in complex biological fluids: (1) desorption of the alkane-thiolate SAM from the surface of the gold electrode;[14−16] (2) irreversible redox reactions degrading the redox reporter;[17] (3) enzymatic degradation of the

Received: June 7, 2021
Accepted: August 25, 2021
Published: September 7, 2021

https://doi.org/10.1021/acssensors.1c01183
ACS Sens. 2021, 6, 3340−3347

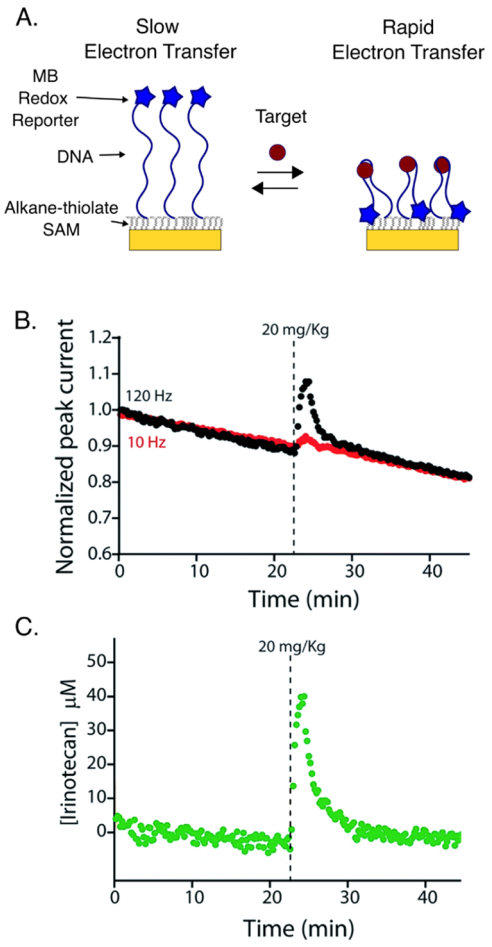

Figure 1. (A) Electrochemical-aptamer based sensors, consisting of redox-reporter-modified aptamers attached to an interrogating electrode via an alkanethiol self-assembled monolayer (SAM), detect their target via a binding-induced change that alters the rate of electron transfer from the electrode. This, in turn, produces an easily measurable signal change when the sensor is interrogated using, for example, square-wave voltammetry.[13] In this study, we used the reporter methylene blue (MB) and a 6-mercaptohexanol monolayer, both of which are commonly employed in in vivo sensor deployments. (B) When EAB sensors are placed within the body, their electrochemical signals drift. Shown here, for example, are signals generated by an irinotecan-detecting EAB sensor placed in the jugular vein of a live rat. The signals were measured at square-wave frequencies of 120 Hz, at which the sensor's response to target is large, and 10 Hz, at which it is small. At 22 min, the rat was dosed with 20 mg/kg intravenous irinotecan resulting in the obvious change in the signal seen at the former frequency. (C) We have historically corrected the drift seen in vivo using kinetic differential measurements (KDM), which corrects drift by taking the difference between these two normalized signals.[11] That is, the electrochemical signal shown in (B) is drift-corrected using KDM and then converted into an estimate of target levels using the previously determined relationship between the KDM signal and the irinotecan concentration. Ultimately, however, the loss in the signal becomes so great that even if the drift can be corrected, the sensor's signal-to-noise ratio begins to fall.[1] In this work, we explore the mechanistic origins of EAB drift in order to ultimately achieve longer duration in vivo measurements. Data in panels B,C are adapted with permission from Idili et al.[8] Copyright (2019) Royal Society of Chemistry.

DNA;[18,19] and (4) fouling from interferents, such as blood cells and proteins, adsorbing to the sensor surface.[20−26] The relative contributions of each of these mechanisms to EAB sensor degradation and drift, however, have not yet been defined, rendering it difficult to develop rational approaches to their remediation. To address this, here we have characterized the relative contributions of each of these mechanisms to the degradation of a simple, EAB-like proxy when exposed in vitro to undiluted whole blood at 37 °C as a straightforward and easily reproducible mimic of in vivo conditions. Specifically, we have employed MB-modified, single-stranded DNA sequences attached via thiol-on-gold monolayer chemistry to a gold electrode, using sequences that lack significant internal complementarity (i.e., that lack secondary or tertiary structure) that might otherwise confound our mechanistic studies by, for example, reducing or enhancing the rate of enzymatic degradation.

When a 37-base, terminally modified EAB-like proxy (MB37) is placed in undiluted whole blood at 37 °C, we observe biphasic loss in the square-wave voltammetry signal arising from its MB (Figure 2A). The first phase is an approximately exponential signal decrease that occurs over ∼1.5 h. This is followed by an approximately linear decrease that occurs over the remaining duration of the experiment. We surmise that the presence of exponential and linear phases occurring on different time scales indicates that at least two distinct mechanisms are contributing to the signal loss seen under these conditions.

To determine whether either of the two, distinct phases are driven by "biology" (i.e., fouling or enzymatic cleavage) or by electrochemistry (i.e., breakage of the gold−thiol bond or irreversible redox reactions of the reporter), we next characterized sensor degradation in a less complex environment: phosphate buffered saline (PBS) at 37 °C (Figure 2B). Under these conditions, the exponential drift phase is effectively abolished, suggesting that it arises due to blood-specific biological mechanisms. The linear phase, in contrast, remains of similar magnitude to the linear phase seen in blood, suggesting that this phase arises due to electrochemical mechanisms. Consistent with this, the drift stops when we pause the electrochemical interrogation in PBS (Figure 3A).

To determine whether the electrochemical mechanism driving the linear phase arises due to monolayer desorption or irreversible reactions of the redox reporter, we next monitored sensor degradation as a function of the potential applied during the square-wave scan. Our argument is that while the stability of the gold−thiol bond is strongly dependent on the applied potential window,[27,28] the stability of the redox reporter is not. Specifically, thiol-on-gold monolayers undergo reductive desorption at potentials below −0.5 V [ref 29], and oxidative desorption occurs at potentials above ∼1 V [ref 27]. In contrast, as long as the potential window includes the potential at which MB oxidizes to the more reactive leucomethylene blue (E_0 = −0.25 V at pH 7.5),[30] any degradation associated with this mechanism would be independent of the width of the potential window. Performing this experiment, we find that the rate of the degradation seen in PBS is strongly dependent on the width of the scan window, thus supporting the hypothesis that it arises from redox-driven breakage of the gold−thiol bond. For example, when we fix the negative side of the potential window at −0.4 V, the degradation rate remains low until the positive side of the potential window exceeds 0.0 V (Figure 3B). Likewise, when we fix the positive side of the potential window at −0.2 V, the degradation rate increases as the negative side of the potential window falls below −0.4 V (Figure 3C). In

https://doi.org/10.1021/acssensors.1c01183
ACS Sens. 2021, 6, 3340−3347

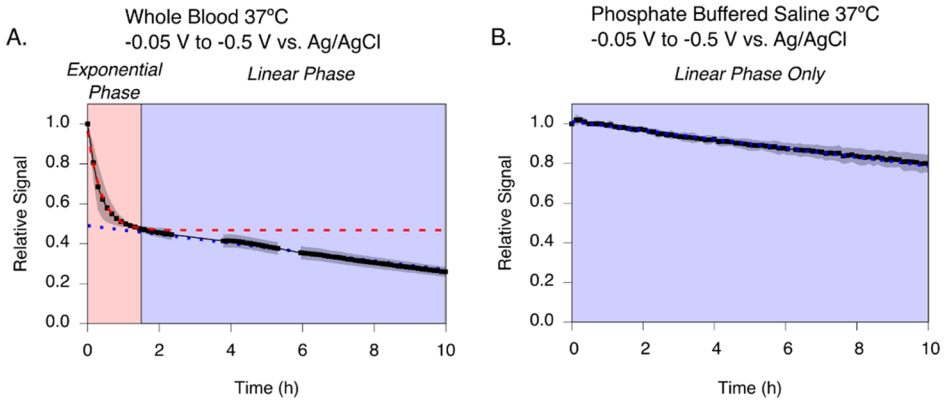

Figure 2. (A) When a simple, EAB-like proxy is placed in whole blood at 37 °C, we observe biphasic loss of the signal. That is, the square-wave peak current observed from the MB reporter decreases in an approximately exponential manner over the first ∼1.5 h (red shading, red dashed line), followed by an effect that is approximately linear in time (blue shading, blue-dotted line). (B) The exponential phase is not seen in PBS at 37 °C, indicating that it is specific to deployment in blood. The linear phase (blue dotted line), in contrast, remains, suggesting that electrochemistry-driven degradation is a major contributor to this phase. Here, we monitored the relative signal via the MB peak observed in square-wave voltammograms scanned from −0.05 to −0.50 V (all potentials reported relative to Ag/AgCl/$Cl^-_{sat'd}$) and using a square-wave frequency of 15 Hz in blood and 20 Hz in PBS. These square-wave frequencies are close to the rate of maximum charge transfer from the MB under the given conditions, and thus reporting more faithfully on the changes in the number of redox reporters present (see Figures S1 and S2). The gray-shaded regions represent standard deviation of four replicate electrodes.

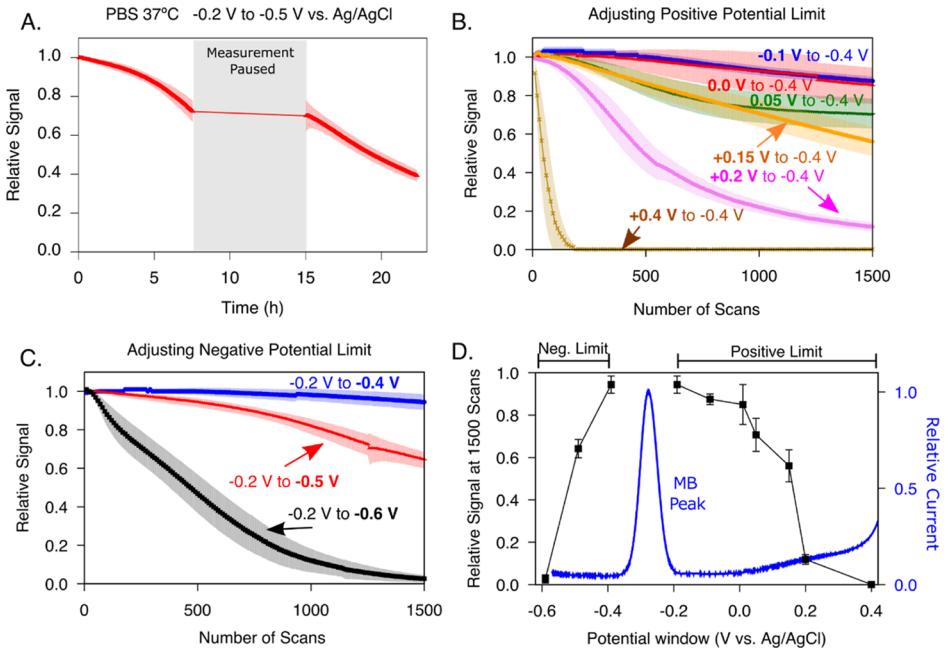

Figure 3. (A) Linear drift phase observed in PBS at 37 °C stops when we pause the potential scanning, thus indicating it is driven by electrochemistry. Consistent with this, the rate of signal degradation seen in PBS is a strong function of the (B) positive and (C) negative limits of the potential windows employed. (D) Specifically, as shown here in black, the signal remaining after 1500 scans [these data are from (B,C)] is dramatically reduced when we hold the negative limit of the scan at −0.4 V and allow the positive limit to climb above 0 V, or when we hold the positive limit at −0.2 V and allow the negative limit to fall below −0.4 V. We believe the former effect arises due to oxidative desorption of the monolayer, which is further exacerbated by the presence of 140 mM chloride in PBS,[31,32] and the latter due to reductive desorption.[29] In contrast, we see almost no degradation in PBS when the potential window is held between −0.4 and −0.2 V (black datapoints), a potential range that coincides fairly closely with the redox peak of MB (blue curve). The shaded regions in panels A−C and error bars in panel D correspond to the standard deviation of n = 4 replicates. Note: as the monolayer desorbs, the degradation rates sometimes varies significantly from electrode to electrode. This is likely due to the nature of the monolayer defects at which degradation is initiated,[33] which depend strongly on the topography of the electrode surface and the characteristics of the monolayer and can easily vary from electrode to electrode.

contrast, when we limit the potential window to −0.4 to −0.2 V, we observe only 5% signal loss after 1500 scans (Figure 3D). The observations here also explain previous reports[17] that sensors employing MB are far more stable than sensors employing any of nearly a dozen other redox reporters: the redox potentials of all of the other redox reporters characterized fall outside of the narrow potential window over which alkane-thiol-on-gold monolayers are stable.

We next explored the mechanisms underlying the biology-driven signal drift, evaluating the relative contributions of enzymatic cleavage of the DNA and fouling. Of note, both mechanisms are expected to "saturate" before complete loss of

https://doi.org/10.1021/acssensors.1c01183
ACS Sens. 2021, 6, 3340−3347

the signal. Specifically, the former saturates due to the relative inaccessibility of some of the DNA strands on the microscopically rough surface,[19] and the latter due to the fact that there are only a finite number of sites for proteins or cells to bind. However, while enzymatic degradation of the DNA is irreversible, fouling is likely at least partially reversible by chemicals that solubilize biomolecules, such as detergents or denaturants.[35−37] We thus washed electrodes that had been interrogated in whole blood for 2.5 h (using a narrow potential window to minimize redox-driven monolayer degradation) with concentrated urea, conditions that do not disrupt the performance of EAB-type devices.[34,38] Doing so, we recovered at least 80% of the initial signal (Figure 4A), suggesting that

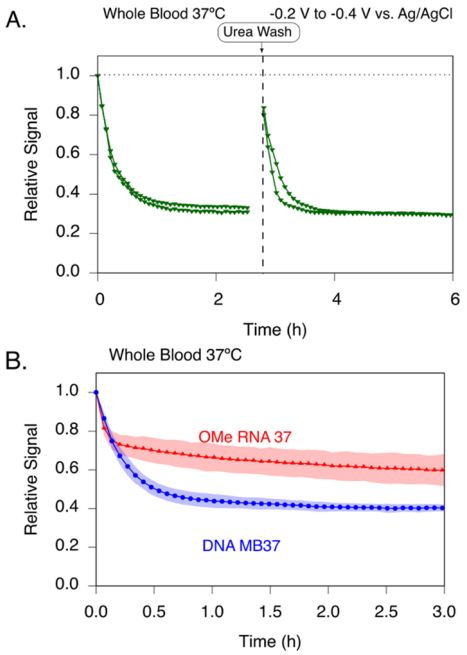

Figure 4. We next investigated whether the exponential drift phase seen in blood arises due to fouling or enzymatic cleavage of the DNA. (A) First, we exposed two electrodes to blood at 37 °C for 2 h using a narrow potential window to minimize the linear drift phase. Washing the electrode with 9.5 M urea, which is expected to largely reverse fouling,[34] recovers the majority of the lost signal. In contrast, such washing cannot reverse enzymatic cleavage of the DNA. (B) Following this, we characterized an enzyme-resistant 2′*O*-methyl analogue of our MB37 DNA construct. Exposing this to whole blood at 37 °C, we once again observe an exponential drift phase. Shading in the latter panel indicates standard deviation of four replicates.

fouling plays a major role in the exponential drift phase. To further explore the potential contributions of enzymatic degradation, we next investigated the drift-properties of an enzyme-resistant 2′*O*-methyl RNA analog of our 37-base DNA construct. Despite the resistance of this non-natural oligonucleotide backbone to DNAse I (Figure S3) and other nucleases,[39,40] this construct also exhibits a significant exponential phase (Figure 4B). This result, which closely parallels recent reports from Arroyo-Currás and co-workers employing enzyme resistant spiegelmers,[41] further supports our argument that fouling dominates the exponential phase.

To better understand the mechanisms by which fouling leads to signal loss, we next characterized the extent to which the rate of electron transfer of the redox reporter varies with the amount of time spent in blood and PBS. To do so, we determined the square-wave voltammetry frequency at which the greatest amount of charge transfer occurs.[42,43] This decreases by a factor of 3 during the exponential drift phase seen in whole blood (Figure 5A), suggesting that fouling is reducing the rate with which the attached MB approaches the electrode surface to transfer electrons.[44] In contrast, the electron transfer rate shifts very little after even 10 h spent in the linear drift regime in PBS (Figure 5B).

The fact that fouling decreases the electron transfer rate (Figure 5A) suggests that it causes drift by altering the dynamics with which the MB reaches the surface to transfer electrons.[44] This, in turn, suggests that the fouling should be sensitive to the position of the MB along the DNA chain.[44] To demonstrate this, we characterized the drift of a series of equal length single-stranded DNAs with the MB reporter placed at various internal positions (Figure 6A). Doing so, we find that the rate of the exponential drift phase is strongly and monotonically dependent on the reporter position (Figure 6B,C). Specifically, the exponential phase is both more rapid and larger in magnitude when the reporter is farther from the electrode surface. This presumably occurs because reporters attached closer to the surface can only transfer electrons to the electrode through a small area near the attachment site,[44] which, due to steric and/or electrostatic repulsion from the DNA chain, is less likely to be blocked by fouling. Reporters attached nearer to the distal end of the DNA, in contrast, normally can reach areas of the electrode surface far from the attachment site, and thus more are affected by the binding of proteins or other fouling components. In contrast, the rate of the linear drift phase is independent of the placement of the reporter (Figure 6D), as would be expected for redox-driven detachment of the DNA from the surface. Consistent with this argument, the drift behavior seen in PBS is likewise effectively independent of the position of the MB (Figure S4).

Although, in order to reduce the potentially confounding effects of the secondary or tertiary structure, we employed unstructured DNA constructs in the above studies, the insights these nevertheless provide guidance toward improving the longevity of EAB sensors employing structured aptamers. To demonstrate this, we challenged a vancomycin-detecting EAB sensor in undiluted whole blood at 37 °C for 24 h using the narrow potential window we identified above to suppress the linear phase and existing drift correction methods[11,12] to correct for the exponential phase. Doing so, we retain good signal to noise throughout the experiment thereby achieving day-long measurements under these challenging conditions. That is, by reducing the width of the potential window and thus eliminating the linear drift phase, square-wave voltammetric peaks obtained at frequencies of 300 and 50 Hz drift in close concert (Figure 7A). Given this, a ratiometric drift correction method[12] (Figure 7B) is sufficient to correct the remaining drift, ensuring that we can measure vancomycin for at least 24 h with clinically relevant (better than ±20%) accuracy and precision (Figure 7C).

DISCUSSION

Here, we have identified the major contributors to the drift produced by the degradation of EAB sensors when they are placed in whole blood at body temperature. The first is a rapid, exponential phase that we have attributed to fouling by blood components. While the complexity of blood renders it difficult to determine which specific components cause this, the recent demonstration that EAB sensors drift similarly in both serum

https://doi.org/10.1021/acssensors.1c01183
ACS Sens. 2021, 6, 3340−3347

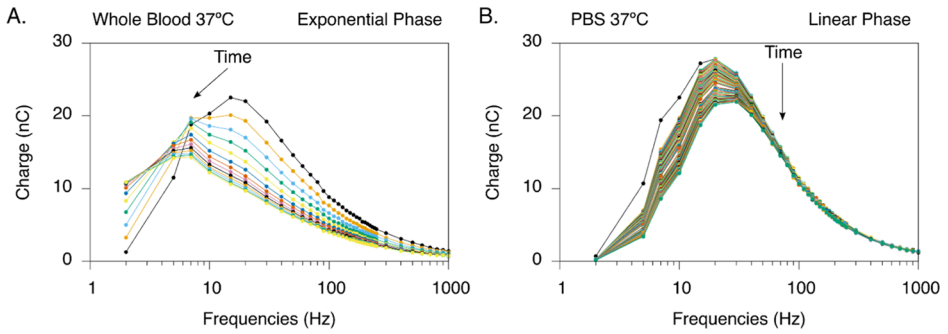

Figure 5. Although the rate of electron transfer shifts significantly during the exponential drift phase, we observe no significant change in the electron transfer rate during the linear phase. Shown are plots of charge transfer as a function of frequency collected over (A) the first 1.5 h in whole blood or (B) over 10 h in PBS for our MB37 DNA construct. During the former, which captures the exponential phase, the rate of electron transfer decreases approximately 3-fold. In contrast, during the latter, much longer linear drift phase, the electron transfer rate shifts very little. These data, which were extracted during the data collection for Figure 2A,B, were collected via square-wave voltammetry performed over the potential window from −0.05 to −0.50 V.

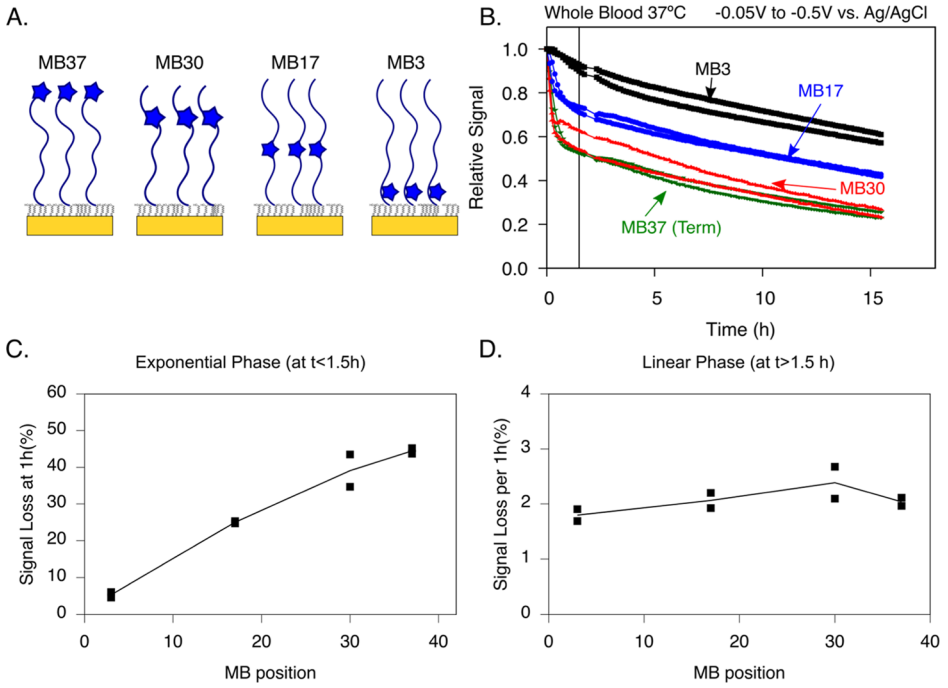

Figure 6. (A) To further characterize the mechanisms underlying drift, we varied the position of the MB redox reporter along single-stranded DNA constructs. (B) Specifically, we placed such constructs in 37 °C undiluted whole blood and monitored the redox signal using square-wave voltammetry performed at the frequency of maximum charge transfer for each construct. (C) Rates associated with the exponential drift phase (denoted here as the loss in signaling current after 1 h) depend strongly on the reporter position. (D) In contrast, the rates associated with the linear drift phase (denoted here as the slopes seen at $t > 2$ h) are effectively independent of reporter placement.

and whole blood[41] suggests that it arises due to proteins rather than cells or clotting factors, as the latter are not present in serum. The second, more-or-less linear phase, which occurs in both blood and PBS, arises due to loss of the reporter-modified DNA via electrochemistry-driven desorption of the monolayer, which can be minimized by narrowing the potential window used in sensor interrogation.

Our results suggest several other approaches to remediating the signal loss seen for EAB and EAB-like electrochemical biosensors when deployed in vivo. For example, in addition to narrowing the potential window, the use of longer-chain monolayers (e.g., an 11-carbon alkanethiolate monolayer[25,45]) would likely also reduce the linear drift phase because they are more electrochemically stable. A potential concern, however, is that thicker monolayers slow electron transfer[46,47] and thus can alter EAB sensor signaling.[25] Likewise, the exponential drift phase can be reduced by employing monolayers that reduce fouling.[48,49] The use of hydrogels and molecular weight cut-off filters that reduce the approach of proteins to the sensor surface may also reduce the magnitude of this drift phase.[50]

The observation that the rate of the exponential drift phase depends on the placement of the redox reporter on the construct sheds light on a previous mystery: why not all square-wave frequencies drift in concert when EAB sensors are placed in biological fluids. Specifically, fouling presumably alters the ease with which the redox reporter accesses the electrode surface, changing in turn its rate of electron transfer and thus differentially affecting the currents observed at any given square-wave frequency. In contrast, loss of the redox reporter via desorption of the SAM, cleavage of the DNA, or

https://doi.org/10.1021/acssensors.1c01183
ACS Sens. 2021, 6, 3340−3347

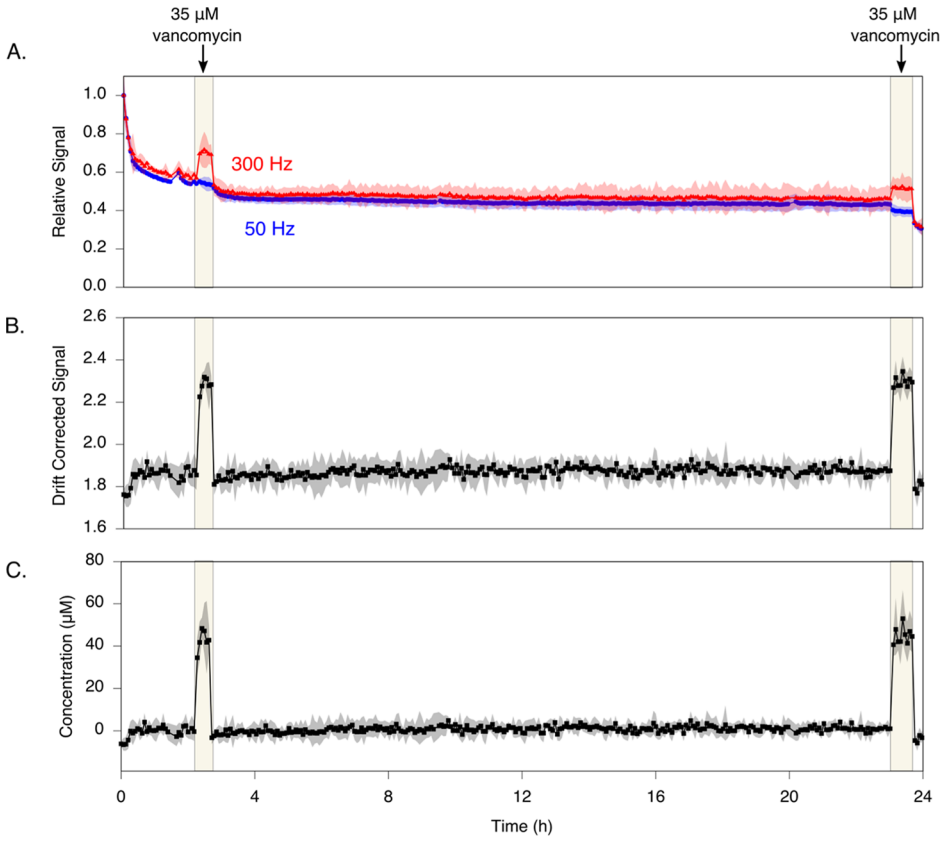

Figure 7. "Lessons learned" from simple, unstructured DNA constructs are directly transferable to EAB sensors. To see this, we challenged a vancomycin-detecting EAB in whole blood at 37 °C with 35 μM additions (beige shading) of vancomycin at 2 and 23 h, using a narrow, −0.2 to −0.4 V potential window. (A) Relative electrochemical signals at square-wave frequencies of 50 and 300 Hz are stable after the first 2 h, suggesting that fouling has saturated by this point, and that the narrow potential window employed here has minimized the linear drift phase. (B) Using a ratiometric drift correction method,[12] where the signal observed at 300 Hz is divided by the signal observed at 50 Hz, the baseline is stable and the signal changes during the two target additions are consistent with each other. (C) By correlating the drift-corrected signal with a calibration curve (Figure S5), the estimated concentrations are likewise relatively precise and with 20% accuracy. The red-, blue-, and gray-shaded regions represent a standard deviation of four replicate electrodes.

irreversible reactions of the MB is expected to cause the same loss in relative signal at all square-wave frequencies. Fortunately, the magnitude and rate of the exponential drift phase depends on both the square-wave frequency employed and the dynamics of both the bound and unbound conformations of the aptamer. Because of this, almost every EAB sensor nevertheless exhibits pairs of frequencies that drift in concert, thus enabling drift correction.[1,6,8,9] For example, using such a matched frequency pair, we demonstrated the ability to perform vancomycin measurements in whole blood at 37 °C without significant diminution of the signal-to-noise ratio and with consistent signal gain (and thus reasonable accuracy and precision) throughout a 24 h measurement run. This suggests that we may be able to achieve similarly long-duration measurements in situ in the living body, improving the utility of EAB sensors as a means of continuously monitoring drugs and biomarkers.

■ ASSOCIATED CONTENT

Supporting Information

The Supporting Information is available free of charge at https://pubs.acs.org/doi/10.1021/acssensors.1c01183.

Materials; description of sensor fabrication, electrochemical measurements, and urea wash; and data on influence of reporter position dependence in PBS, enzymatic resistance of 2′*O*-methyl RNA, and the calibration of the vancomycin-detecting sensor (PDF)

■ AUTHOR INFORMATION

Corresponding Author

Kevin W. Plaxco − *Department of Chemistry and Biochemistry, University of California Santa Barbara, Santa Barbara, California 93106, United States; Center for Bioengineering and Department of Mechanical Engineering, University of California Santa Barbara, Santa Barbara, California 93106, United States;* orcid.org/0000-0003-4772-8771; Email: kwp@ucsb.edu

Authors

Kaylyn K. Leung − *Department of Chemistry and Biochemistry, University of California Santa Barbara, Santa Barbara, California 93106, United States; Center for Bioengineering, University of California Santa Barbara, Santa Barbara, California 93106, United States;* orcid.org/0000-0002-8966-801X

Alex M. Downs − *Center for Bioengineering and Department of Mechanical Engineering, University of California Santa Barbara, Santa Barbara, California 93106, United States*

Gabriel Ortega − *Department of Chemistry and Biochemistry, University of California Santa Barbara, Santa Barbara,*

https://doi.org/10.1021/acssensors.1c01183
ACS Sens. 2021, 6, 3340−3347

California 93106, United States; Center for Bioengineering, University of California Santa Barbara, Santa Barbara, California 93106, United States; orcid.org/0000-0002-7126-9096

Martin Kurnik − *Department of Chemistry and Biochemistry, University of California Santa Barbara, Santa Barbara, California 93106, United States; Center for Bioengineering, University of California Santa Barbara, Santa Barbara, California 93106, United States;* orcid.org/0000-0001-9255-9730

Complete contact information is available at: https://pubs.acs.org/10.1021/acssensors.1c01183

Notes

The authors declare the following competing financial interest(s): The authors declare the following competing financial interest(s): One author (K. W. P.) has a financial interest in and serves on the scientific advisory boards of two companies attempting to commercialize E-AB sensors.

■ ACKNOWLEDGMENTS

We thank Prof. Justin Gooding for helpful advice, suggestions, and discussion of experiments regarding fouling and enzymatic cleavage. We also thank Prof. Philippe Dauphin-Ducharme for interpretation of electrochemical signals for DNA internally modified with methylene blue. This work was supported by the NIH (R01AI145206), by the Office of Naval Research (N00014-20-1-2164), by the Otis Williams Postdoctoral Fellowship Fund (K.L.), and the National Science Foundation Graduate Research Fellowship under grant no. 1650114 (A.D.).

■ REFERENCES

(1) Arroyo-Currás, N.; Somerson, J.; Vieira, P. A.; Ploense, K. L.; Kippin, T. E.; Plaxco, K. W. Real-Time Measurement of Small Molecules Directly in Awake, Ambulatory Animals. *Proc. Natl. Acad. Sci. U.S.A.* **2017**, *114*, 645−650.

(2) Das, J.; Cederquist, K. B.; Zaragoza, A. A.; Lee, P. E.; Sargent, E. H.; Kelley, S. O. An Ultrasensitive Universal Detector Based on Neutralizer Displacement. *Nat. Chem.* **2012**, *4*, 642−648.

(3) Patolsky, F.; Weizmann, Y.; Willner, I. Redox-Active Nucleic-Acid Replica for the Amplified Bioelectrocatalytic Detection of Viral DNA. *J. Am. Chem. Soc.* **2002**, *124*, 770−772.

(4) Hansen, J. A.; Mukhopadhyay, R.; Hansen, J. Ø.; Gothelf, K. V. Femtomolar Electrochemical Detection of DNA Targets Using Metal Sulfide Nanoparticles. *J. Am. Chem. Soc.* **2006**, *128*, 3860−3861.

(5) Gooding, J. J. Electrochemical DNA Hybridization Biosensors. *Electroanalysis* **2002**, *14*, 1149−1156.

(6) Dauphin-Ducharme, P.; Yang, K.; Arroyo-Currás, N.; Ploense, K. L.; Zhang, Y.; Gerson, J.; Kurnik, M.; Kippin, T. E.; Stojanovic, M. N.; Plaxco, K. W. Electrochemical Aptamer-Based Sensors for Improved Therapeutic Drug Monitoring and High-Precision, Feedback-Controlled Drug Delivery. *ACS Sensors* **2019**, *4*, 2832−2837.

(7) Arroyo-Currás, N.; Ortega, G.; Copp, D. A.; Ploense, K. L.; Plaxco, Z. A.; Kippin, T. E.; Hespanha, J. P.; Plaxco, K. W. High-Precision Control of Plasma Drug Levels Using Feedback-Controlled Dosing. *ACS Pharmacol. Transl. Sci.* **2018**, *1*, 110−118.

(8) Idili, A.; Arroyo-Currás, N.; Ploense, K. L.; Csordas, A. T.; Kuwahara, M.; Kippin, T. E.; Plaxco, K. W. Seconds-Resolved Pharmacokinetic Measurements of the Chemotherapeutic Irinotecan: In Situ in the Living Body. *Chem. Sci.* **2019**, *10*, 8164−8170.

(9) Idili, A.; Gerson, J.; Kippin, T.; Plaxco, K. W. Seconds-Resolved, In Situ Measurements of Plasma Phenylalanine Disposition Kinetics in Living Rats. *Anal. Chem.* **2021**, *93*, 4023.

(10) Rawson, T. M.; O'Hare, D.; Herrero, P.; Sharma, S.; Moore, L. S. P.; de Barra, E.; Roberts, J. A.; Gordon, A. C.; Hope, W.; Georgiou, P.; et al. Delivering Precision Antimicrobial Therapy through Closed-Loop Control Systems. *J. Antimicrob. Chemother.* **2018**, *73*, 835−843.

(11) Ferguson, B. S.; Hoggarth, D. A.; Maliniak, D.; Ploense, K.; White, R. J.; Woodward, N.; Hsieh, K.; Bonham, A. J.; Eisenstein, M.; Kippin, T. E.; et al. Real-Time, Aptamer-Based Tracking of Circulating Therapeutic Agents in Living Animals. *Sci. Transl. Med.* **2013**, *5*, 213ra165.

(12) Li, H.; Dauphin-Ducharme, P.; Ortega, G.; Plaxco, K. W. Calibration-Free Electrochemical Biosensors Supporting Accurate Molecular Measurements Directly in Undiluted Whole Blood. *J. Am. Chem. Soc.* **2017**, *139*, 11207−11213.

(13) White, R. J.; Rowe, A. A.; Plaxco, K. W. Re-Engineering Aptamers to Support Reagentless, Self-Reporting Electrochemical Sensors. *Analyst* **2010**, *135*, 589.

(14) Flynn, N. T.; Tran, T. N. T.; Cima, M. J.; Langer, R. Long-Term Stability of Self-Assembled Monolayers in Biological Media. *Langmuir* **2003**, *19*, 10909−10915.

(15) Poirier, G. E.; Tarlov, M. J.; Rushmeier, H. E. Two-Dimensional Liquid Phase and the px.sqroot.3 Phase of Alkanethiol Self-Assembled Monolayers on Au(111). *Langmuir* **1994**, *10*, 3383−3386.

(16) Xu, X.; Makaraviciute, A.; Kumar, S.; Wen, C.; Sjödin, M.; Abdurakhmanov, E.; Danielson, U. H.; Nyholm, L.; Zhang, Z. Structural Changes of Mercaptohexanol Self-Assembled Monolayers on Gold and Their Influence on Impedimetric Aptamer Sensors. *Anal. Chem.* **2019**, *91*, 14697−14704.

(17) Kang, D.; Ricci, F.; White, R. J.; Plaxco, K. W. Survey of Redox-Active Moieties for Application in Multiplexed Electrochemical Biosensors. *Anal. Chem.* **2016**, *88*, 10452−10458.

(18) Deng, M.; Li, M.; Li, F.; Mao, X.; Li, Q.; Shen, J.; Fan, C.; Zuo, X. Programming Accessibility of DNA Monolayers for Degradation-Free Whole-Blood Biosensors. *ACS Mater. Lett.* **2019**, *1*, 671−676.

(19) Biagiotti, V.; Porchetta, A.; Desiderati, S.; Plaxco, K. W.; Palleschi, G.; Ricci, F. Probe Accessibility Effects on the Performance of Electrochemical Biosensors Employing DNA Monolayers. *Anal. Bioanal. Chem.* **2012**, *402*, 413−421.

(20) Li, Z.; Jin, R.; Mirkin, C. A.; Letsinger, R. L. Multiple Thiol-Anchor Capped DNA-Gold Nanoparticle Conjugates. *Nucleic Acids Res.* **2002**, *30*, 1558−1562.

(21) Jia, Y.; Wei, B.; Duan, R.; Zhang, Y.; Wang, B.; Hakeem, A.; Liu, N.; Ou, X.; Xu, S.; Chen, Z.; et al. Imparting Biomolecules to a Metal-Organic Framework Material by Controlled DNA Tetrahedron Encapsulation. *Sci. Rep.* **2015**, *4*, 5929.

(22) Ma, J.; Chai, W.; Lu, J.; Tian, T.; Wu, S.; Yang, Y.; Yang, J.; Li, C.; Li, G. Coating a DNA Self-Assembled Monolayer with a Metal Organic Framework-Based Exoskeleton for Improved Sensing Performance. *Analyst* **2019**, *144*, 3539−3545.

(23) Hu, B.; Kong, F.; Gao, X.; Jiang, L.; Li, X.; Gao, W.; Xu, K.; Tang, B. Avoiding Thiol Compound Interference: A Nanoplatform Based on High-Fidelity Au−Se Bonds for Biological Applications. *Angew. Chem., Int. Ed.* **2018**, *57*, 5306−5309.

(24) Ricci, F.; Zari, N.; Caprio, F.; Recine, S.; Amine, A.; Moscone, D.; Palleschi, G.; Plaxco, K. W. Surface Chemistry Effects on the Performance of an Electrochemical DNA Sensor. *Bioelectrochemistry* **2009**, *76*, 208−213.

(25) Lai, R. Y.; Seferos, D. S.; Heeger, A. J.; Bazan, G. C.; Plaxco, K. W. Comparison of the Signaling and Stability of Electrochemical DNA Sensors Fabricated from 6- or 11-Carbon Self-Assembled Monolayers. *Langmuir* **2006**, *22*, 10796−10800.

(26) Phares, N.; White, R. J.; Plaxco, K. W. Improving the Stability and Sensing of Electrochemical Biosensors by Employing Trithiol-Anchoring Groups in a Six-Carbon Self-Assembled Monolayer. *Anal. Chem.* **2009**, *81*, 1095−1100.

(27) Widrig, C. A.; Chung, C.; Porter, M. D. The Electrochemical Desorption of N-Alkanethiol Monolayers from Polycrystalline Au and Ag Electrodes. *J. Electroanal. Chem. Interfacial Electrochem.* **1991**, *310*, 335−359.

(28) Zhong, C.-J.; Porter, M. D. Fine Structure in the Voltammetric Desorption Curves of Alkanethiolate Monolayers Chemisorbed at Gold. *J. Electroanal. Chem.* **1997**, *425*, 147−153.
(29) Wackerbarth, H.; Grubb, M.; Zhang, J.; Hansen, A. G.; Ulstrup, J. Long-Range Order of Organized Oligonucleotide Monolayers on Au(111) Electrodes. *Langmuir* **2004**, *20*, 1647−1655.
(30) Tani, A.; Thomson, A. J.; Butt, J. N. Methylene Blue as an Electrochemical Discriminator of Single-and Double-Stranded Oligonucleotides Immobilised on Gold Substrates. *Analyst* **2001**, *126*, 1756−1759.
(31) Ye, S.; Ishibashi, C.; Uosaki, K. Anisotropic Dissolution of an Au(111) Electrode in Perchloric Acid Solution Containing Chloride Anion Investigated by in Situ STM-The Important Role of Adsorbed Chloride Anion. *Langmuir* **1999**, *15*, 807−812.
(32) Zamborini, F. P.; Crooks, R. M. Corrosion Passivation of Gold by N-Alkanethiol Self-Assembled Monolayers: Effect of Chain Length and End Group. *Langmuir* **1998**, *14*, 3279−3286.
(33) Wano, H.; Uosaki, K. In Situ, Real-Time Monitoring of the Reductive Desorption Process of Self-Assembled Monolayers of Hexanethiol on Au(111) Surfaces in Acidic and Alkaline Aqueous Solutions by Scanning Tunneling Microscopy. *Langmuir* **2001**, *17*, 8224−8228.
(34) Kurnik, M.; Ortega, G.; Dauphin-Ducharme, P.; Li, H.; Caceres, A.; Plaxco, K. W. Quantitative Measurements of Protein−surface Interaction Thermodynamics. *Proc. Natl. Acad. Sci. U.S.A.* **2018**, *115*, 8352−8357.
(35) Sanawar, H.; Pinel, I.; Farhat, N. M.; Bucs, Sz. S.; Zlopasa, J.; Kruithof, J. C.; Witkamp, G. J.; van Loosdrecht, M. C. M.; Vrouwenvelder, J. S. Enhanced biofilm solubilization by urea in reverse osmosis membrane systems. *Water Research X* **2018**, *1*, 100004.
(36) Sanawar, H.; Bucs, S. S.; Pot, M. A.; Zlopasa, J.; Farhat, N. M.; Witkamp, G.-J.; Kruithof, J. C.; van Loosdrecht, M. C. M.; Vrouwenvelder, J. S. Pilot-Scale Assessment of Urea as a Chemical Cleaning Agent for Biofouling Control in Spiral-Wound Reverse Osmosis Membrane Elements. *Membranes* **2019**, *9*, 117.
(37) Hlady, V.; Buijs, J.; Jennissen, H. P. Methods for Studying Protein Adsorption. *Methods Enzymol.* **1999**, *309*, 402−429.
(38) Watkins, H. M.; Vallée-Bélisle, A.; Ricci, F.; Makarov, D. E.; Plaxco, K. W. Entropic and Electrostatic Effects on the Folding Free Energy of a Surface-Attached Biomolecule: An Experimental and Theoretical Study. *J. Am. Chem. Soc.* **2012**, *134*, 2120−2126.
(39) Burmeister, P. E.; Lewis, S. D.; Silva, R. F.; Preiss, J. R.; Horwitz, L. R.; Pendergrast, P. S.; McCauley, T. G.; Kurz, J. C.; Epstein, D. M.; Wilson, C.; et al. Direct in Vitro Selection of a 2′-O-Methyl Aptamer to VEGF. *Chem. Biol.* **2005**, *12*, 25−33.
(40) Liu, Z.; Chen, T.; Romesberg, F. E. Evolved Polymerases Facilitate Selection of Fully 2′-OMe-Modified Aptamers. *Chem. Sci.* **2017**, *8*, 8179−8182.
(41) Shaver, A.; Kundu, N.; Young, B. E.; Vieira, P. A.; Sczepanski, J. T.; Arroyo-Currás, N. Nuclease Hydrolysis Does Not Drive the Rapid Signaling Decay of DNA Aptamer-Based Electrochemical Sensors in Biological Fluids. *Langmuir* **2021**, *37*, 5213−5221.
(42) Komorsky-Lovrić, Š.; Lovrić, M. Measurements of Redox Kinetics of Adsorbed Azobenzene by "a Quasireversible Maximum" in Square-Wave Voltammetry. *Electrochim. Acta* **1995**, *40*, 1781−1784.
(43) Dauphin-Ducharme, P.; Arroyo-Currás, N.; Plaxco, K. W. High-Precision Electrochemical Measurements of the Guanine-, Mismatch-, and Length-Dependence of Electron Transfer from Electrode-Bound DNA Are Consistent with a Contact-Mediated Mechanism. *J. Am. Chem. Soc.* **2019**, *141*, 1304−1311.
(44) Dauphin-Ducharme, P.; Arroyo-Currás, N.; Adhikari, R.; Somerson, J.; Ortega, G.; Makarov, D. E.; Plaxco, K. W. Chain Dynamics Limit Electron Transfer from Electrode-Bound, Single-Stranded Oligonucleotides. *J. Phys. Chem. C* **2018**, *122*, 21441−21448.
(45) Love, J. C.; Estroff, L. A.; Kriebel, J. K.; Nuzzo, R. G.; Whitesides, G. M. Self-Assembled Monolayers of Thiolates on Metals as a Form of Nanotechnology. *Chem. Rev.* **2005**, *105*, 1103−1170.
(46) Salomon, A.; Cahen, D.; Lindsay, S.; Tomfohr, J.; Engelkes, V. B.; Frisbie, C. D. Comparison of Electronic Transport Measurements on Organic Molecules. *Adv. Mater.* **2003**, *15*, 1881−1890.
(47) Scaini, D.; Castronovo, M.; Casalis, L.; Scoles, G. Electron Transfer Mediating Properties of Hydrocarbons as a Function of Chain Length: A Differential Scanning Conductive Tip Atomic Force Microscopy Investigation. *ACS Nano* **2008**, *2*, 507−515.
(48) Li, H.; Dauphin-Ducharme, P.; Arroyo-Currás, N.; Tran, C. H.; Vieira, P. A.; Li, S.; Shin, C.; Somerson, J.; Kippin, T. E.; Plaxco, K. W. A Biomimetic Phosphatidylcholine-Terminated Monolayer Greatly Improves the In Vivo Performance of Electrochemical Aptamer-Based Sensors. *Angew. Chem., Int. Ed.* **2017**, *56*, 7492−7495.
(49) Zhang, J.; Lao, R.; Song, S.; Yan, Z.; Fan, C. Design of an Oligonucleotide-Incorporated Nonfouling Surface and Its Application in Electrochemical DNA Sensors for Highly Sensitive and Sequence-Specific Detection of Target DNA. *Anal. Chem.* **2008**, *80*, 9029−9033.
(50) Santos-Cancel, M.; White, R. J. Collagen Membranes with Ribonuclease Inhibitors for Long-Term Stability of Electrochemical Aptamer-Based Sensors Employing RNA. *Anal. Chem.* **2017**, *89*, 5598−5604.

https://doi.org/10.1021/acssensors.1c01183
ACS Sens. 2021, 6, 3340−3347